A subwavelength slit as a quarter-wave retarder

Philip F. Chimento,[1,*] Nikolay V. Kuzmin,[1,2] Johan Bosman,[1]
Paul F. A. Alkemade,[3] Gert W. 't Hooft,[1,4] and Eric R. Eliel[1]

[1]Huygens Laboratory, Leiden University, P. O. Box 9504, 2300 RA Leiden, Netherlands
[2]Current address: Department of Physics and Astronomy, Faculty of Sciences, VU University Amsterdam, De Boelelaan 1105, 1081 HV Amsterdam, Netherlands
[3]Kavli Institute of Nanoscience, Delft University of Technology, Lorentzweg 1, 2628 CJ Delft, Netherlands
[4]Philips Research Laboratories, Prof. Holstlaan 4, 5656 AA Eindhoven, Netherlands
[*]chimento@physics.leidenuniv.nl

Abstract: We have experimentally studied the polarization-dependent transmission properties of a nanoslit in a gold film as a function of its width. The slit exhibits strong birefringence and dichroism. We find, surprisingly, that the transmission of the polarization parallel to the slit only disappears when the slit is much narrower than half a wavelength, while the transmission of the perpendicular component is reduced by the excitation of surface plasmons. We exploit the slit's dichroism and birefringence to realize a quarter-wave retarder.

OCIS codes: (310.6628) Subwavelength structure, nanostructures; (230.7370) Waveguides; (260.1440) Birefringence; (050.1930) Dichroism; (240.6680) Surface plasmons.

References and links

1. Lord Rayleigh, "On the passage of waves through apertures in plane screens, and allied problems," Philos. Mag. **43**, 259–272 (1897).
2. H. A. Bethe, "Theory of diffraction by small holes," Phys. Rev. **66**, 163–182 (1944).
3. C. J. Bouwkamp, "Diffraction theory," Rep. Prog. Phys. **17**, 35–100 (1954).
4. R. V. Jones and J. C. S. Richards, "The polarization of light by narrow slits," Proc. R. Soc. London A **225**, 122–135 (1954).
5. G. Bouwhuis, J. Braat, A. Huijser, J. Pasman, G. van Rosmalen, and K. Schouhamer Immink, *Principles of Optical Disk Systems* (Adam Hilger Ltd., Bristol, 1985).
6. M. H. Fizeau, "Recherches sur plusieurs phénomènes relatifs à la polarisation de la lumière," Annal. Chim. Phys. **63**, 385 (1861).
7. T. W. Ebbesen, H. J. Lezec, H. F. Ghaemi, T. Thio, and P. A. Wolff, "Extraordinary optical transmission through sub-wavelength hole arrays," Nature (London) **391**, 667–669 (1998).
8. S. Astilean, P. Lalanne, and M. Palamaru, "Light transmission through metallic channels much smaller than the wavelength," Opt. Commun. **175**, 265–273 (2000).
9. Y. Takakura, "Optical resonance in a narrow slit in a thick metallic screen," Phys. Rev. Lett. **86**, 5601 (2001).
10. F. Yang and J. R. Sambles, "Resonant transmission of microwaves through a narrow metallic slit," Phys. Rev. Lett. **89**, 063901 (2002).
11. J. R. Suckling, A. P. Hibbins, M. J. Lockyear, T. W. Preist, J. R. Sambles, and C. R. Lawrence, "Finite conductance governs the resonance transmission of thin metal slits at microwave frequencies," Phys. Rev. Lett. **92**, 147401 (2004).
12. H. F. Schouten, T. D. Visser, D. Lenstra, and H. Blok, "Light transmission through a subwavelength slit: waveguiding and optical vortices," Phys. Rev. E **67**, 036608 (2003).
13. H. F. Schouten, T. D. Visser, G. Gbur, D. Lenstra, and H. Blok, "The diffraction of light by narrow slits in plates of different materials," J. Opt. A **6**, S277–S280 (2004).

#154733 - $15.00 USD Received 16 Sep 2011; revised 28 Oct 2011; accepted 2 Nov 2011; published 14 Nov 2011

14. H. F. Schouten, N. Kuzmin, G. Dubois, T. D. Visser, G. Gbur, P. F. A. Alkemade, H. Blok, G. W. 't Hooft, D. Lenstra, and E. R. Eliel, "Plasmon-assisted two-slit transmission: Young's experiment revisited," Phys. Rev. Lett. **94**, 053901 (2005).
15. P. Lalanne, J. P. Hugonin, and J. C. Rodier, "Approximate model for surface-plasmon generation at slit apertures," J. Opt. Soc. Am. A **23**, 1608–1615 (2006).
16. A.-L. Baudrion, F. de León-Pérez, O. Mahboub, A. Hohenau, H. Ditlbacher, F. J. García-Vidal, J. Dintinger, T. W. Ebbesen, L. Martín-Moreno, and J. R. Krenn, "Coupling efficiency of light to surface plasmon polariton for single subwavelength holes in a gold film," Opt. Express **16**, 3420–3429 (2008).
17. H. W. Kihm, K. G. Lee, D. S. Kim, J. H. Kang, and Q.-H. Park, "Control of surface plasmon generation efficiency by slit-width tuning," Appl. Phys. Lett. **92**, 051115 (2008).
18. A. M. Nugrowati, S. F. Pereira, and A. S. van de Nes, "Near and intermediate fields of an ultrashort pulse transmitted through Young's double-slit experiment," Phys. Rev. A **77**, 053810 (2008).
19. A. W. Snyder and J. D. Love, *Optical Waveguide Theory* (Chapman & Hall, London, 1983).
20. E. H. Khoo, E. P. Li, and K. B. Crozier, "Plasmonic wave plate based on subwavelength nanoslits," Opt. Lett. **36**, 2498–2500 (2011).

1. Introduction

The study of the transmission of light through small perforations in metal films has a venerable history [1–4] and has important applications in the field of optical data storage [5]. It dates back to the middle of the nineteenth century when Fizeau described the polarizing effect of wedge-shaped scratches in such films [6].

This field has recently come back to center stage following the observation that, at a specific set of wavelengths, the transmission of a thin metal film containing a regular two-dimensional array of subwavelength apertures is much larger than elementary diffraction theory predicts [7]. This phenomenon of extraordinary optical transmission, which is commonly attributed to surface plasmons traveling along the corrugated interface, has spawned many studies of thin metal films carrying variously-shaped corrugations and perforations. These include holes with circular, cylindrical, or rectangular cross sections [8], either individually or in arrays, and elongated slits [9–11]. The polarization of the incident light is an important parameter, in particular when the width of the hole or slit is subwavelength in one or both directions. The case of a slit which is long in one dimension and subwavelength in the other seems particularly simple, as elementary waveguide theory predicts that it acts as a perfect polarizer when the slit width is less than about half the wavelength of the incident light.

For infinitely long slits, one can define transverse electric (TE) and transverse magnetic (TM) polarized modes. The TM mode's electric field vector is perpendicular to the long axis of the slit, and the TE mode has its electric field vector parallel to the long axis. In standard waveguide models, the metal is usually assumed to be perfect, so that the continuity equation for the electric field implies that its parallel component must be zero at the metallic boundaries. In a slit geometry, this implies that TE-polarized light incident on such a slit will not be transmitted by the structure if the wavelength λ of the incident light is larger than twice the slit width w. This width is commonly referred to as the cutoff width. The TM-polarized mode, on the other hand, can propagate unimpeded through the slit, the effective mode index increasing steadily as the width is reduced [8, 9]. For this reason one expects very narrow slits in metal films to act as perfect polarizers [6].

While the perfect metal model is an excellent approximation for wavelengths in the mid to far infrared or microwave domains, the model is too naïve when the wavelength of the incident light is smaller, because of the dispersion in the permittivity of metals. As a consequence, in the visible part of the spectrum the TE mode cutoff width of real metals like silver and aluminum is slightly smaller than $\lambda/2$ [12, 13], and the cutoff is more gradual. Although the TM mode propagates through the slit, it couples to surface plasmon modes on the front and back surfaces of the slit [14], which act as a loss channel. Since these losses are larger for

#154733 - $15.00 USD Received 16 Sep 2011; revised 28 Oct 2011; accepted 2 Nov 2011; published 14 Nov 2011

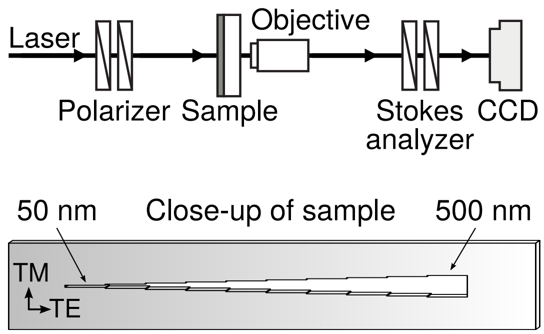

Fig. 1. Sketch of the experimental setup. The sample, which consists of a 200 nm gold film sputtered on top of a glass substrate, is illuminated on the gold side. The transmitted light's polarization is analyzed for each pixel of a CCD camera. The Stokes analyzer consists of a quarter-wave plate and a linear polarizer, which can be rotated independently of each other under computer control to any desired orientation.

certain slit widths [15–17], the transmitted intensity of the TM mode is more dependent on the slit width than the perfectly conducting waveguide model predicts.

Here we demonstrate that, for thin metal films, a nanoslit acts as a lossy optical retarder, and that the TE/TM transmission ratio is around unity well below the cutoff width, approaching zero only when the slit is extremely narrow. We have employed these properties to turn such a slit into a quarter-wave retarder.

2. Description of experiment

In the experiment, shown schematically in Fig. 1, we illuminate an array of ten 10 µm by 50–500 nm slits with a laser beam at $\lambda = 830$ nm, at normal incidence. For all practical purposes, each slit's length can be considered infinite compared to its width and the laser wavelength. The slits are milled through a 200 nm thick gold film using a focused Ga^+ ion beam. The slits' widths increase stepwise from 50 nm, well below the cutoff width for TE-polarized light, to 500 nm, at which value the lowest TE mode can propagate through the slit. The film is deposited on a 0.5 mm thick Schott D263T borosilicate glass substrate, covered by a 10 nm titanium adhesion layer which damps surface plasmons, ensuring that their propagation length is negligibly short on the gold-air interface.

The laser beam width at the sample is approximately 4 mm so that, effectively, the sample is illuminated homogeneously with a flat wavefront. The light transmitted by the structure is imaged on a CCD camera (Apogee Alta U1) by means of a 0.65 NA microscope objective. The polarization of the light incident on the structure is controlled by a combination of half-wave and quarter-wave plates, enabling us to perform the experiment with a variety of input polarizations.

We perform a polarization analysis on the transmitted light, which consists of measuring its Stokes parameters for each slit using a quarter-wave plate and a linear polarizer. We define the Stokes parameters as follows: S_0 is the total intensity, S_1 is the intensity of the horizontal linear component (TE) minus the intensity of the vertical linear component (TM), S_2 is the intensity of the diagonal (45° clockwise) linear component minus the intensity of the anti-diagonal (45° counterclockwise) linear component, and S_3 is the intensity of the right-handed circular component minus the intensity of the left-handed circular component. Since the transmitted light is fully polarized, it is convenient to use the *normalized* Stokes parameters $s_1 = S_1/S_0$, $s_2 = S_2/S_0$, and $s_3 = S_3/S_0$, so that each ranges from -1 to $+1$.

#154733 - $15.00 USD Received 16 Sep 2011; revised 28 Oct 2011; accepted 2 Nov 2011; published 14 Nov 2011

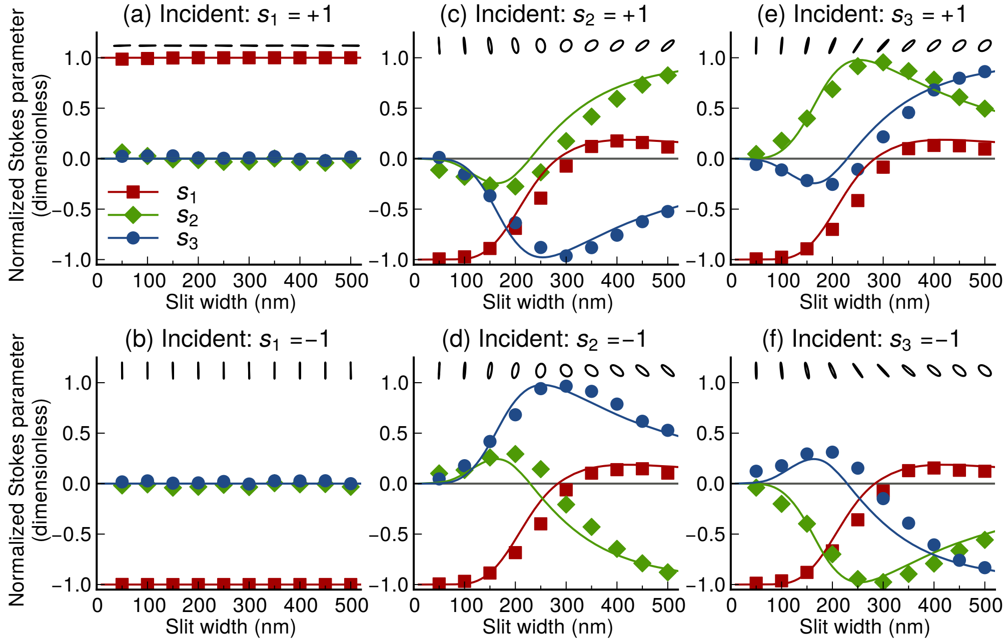

Fig. 2. Normalized Stokes parameters of the light transmitted through the slit, for illumination with (a) horizontal linear polarization ($s_1 = +1$), (b) vertical linear polarization ($s_1 = -1$), (c) diagonal linear polarization ($s_2 = +1$), (d) antidiagonal linear polarization ($s_2 = -1$), (e) left-handed circular polarization ($s_3 = +1$), and (f) right-handed circular polarization ($s_3 = -1$). The polarization ellipses above each graph provide a quick visual indication of the polarization state of the transmitted light. The solid lines represent the results of our model based on simple waveguide theory.

3. Results and interpretation

The full Stokes analysis of the transmitted light, for each of the six basic Stokes input polarizations ($s_{1,2,3} = \pm 1$), is shown in Fig. 2. Figures 2a–b confirm that the TE and TM directions are the slit's eigenpolarizations. Each has its own damping and propagation constant. In the general case, a slit is therefore both dichroic and birefringent, both properties depending on the slit width w.

Looking at Figs. 2c–f, we see that s_1 goes to -1 as the slit gets narrower, for nontrivial input polarizations. The TM polarization is transmitted much more easily through the narrowest slits, since there the transmitted polarization is dominated by TM for any input polarization.

Let us examine Figs. 2c–d more closely, where the incident wave is diagonally linearly polarized ($s_2 = \pm 1$). As the slit width w is reduced from 500 to 300 nm, the transmitted light gradually becomes more and more elliptically polarized, while the main axis of the polarization ellipse remains oriented along the polarization direction of the incident light. As w is reduced further to around 250 nm, the transmitted polarization assumes a more circular form. For narrower slits, the polarization ellipse orients itself essentially vertically, and the polarization becomes more linear, ultimately being purely TM-polarized at $w = 50$ nm. In Figs. 2e–f, a similar process happens as w is reduced, except that the transmitted polarization changes gradually from almost circular to linear, before becoming nearly TM-polarized at $w = 50$ nm.

We note that there is a point in Figs. 2e–f, around $w \approx 250$ nm, where circular polarization is transformed into linear polarization. This implies that the slit acts as a quarter-wave retarder,

#154733 - $15.00 USD Received 16 Sep 2011; revised 28 Oct 2011; accepted 2 Nov 2011; published 14 Nov 2011

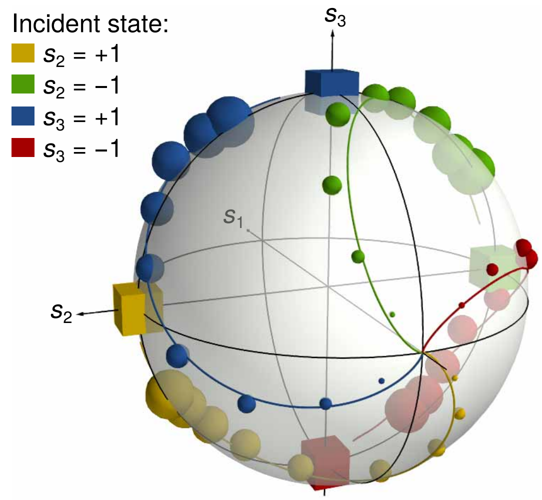

Fig. 3. Path of the transmitted polarization state over the Poincaré sphere as the slit width decreases. The incident polarization state starts at one of the poles or equatorial points, represented by the boxlike markers. The spherical markers, with size proportional to the slit width, mark the transmitted polarization state as it travels over the sphere's surface. The solid lines are the predictions of our model.

albeit with unequal losses for the fast and slow axes. Because of the inequality of these losses, the incident diagonal polarization in Figs. 2c–d is not transformed into a perfectly circular polarization. However, a properly oriented linear polarization incident on a $w \approx 250$ nm slit whose orientation compensates for the differential loss, *will* be transformed into circular polarization. Experiments on other slits have shown that the measured dichroism is highly dependent on the slit parameters and the incident wavelength. Measurements indicate that the polarization-dependent loss can also weakly depend on the detector's numerical aperture. Realizing an ideal quarter-wave retarder therefore requires careful design and manufacture of the slit and the experiment, or serendipity.

As expected, the curves of s_2 and s_3 as a function of w flip their sign when the sign of the incident Stokes parameter is flipped. When the incident light's s_2 and s_3 are exchanged, on the other hand, so are s_2 and s_3 in the transmitted light. The curve of s_1 remains the same for all non-s_1 incident polarizations. The results shown in Fig. 2 can all be represented in one figure by plotting the measured Stokes parameters on the Poincaré sphere. The reduction of the slit width then represents a path of the transmitted polarization state over the Poincaré sphere's surface, as shown in Fig. 3.

In order to analyze our experimental data, we write the incident field as a Jones vector, preceded by an arbitrary complex amplitude such that the TE component is real and positive:

$$\mathbf{E}_{\text{in}} = \tilde{A} \begin{bmatrix} E_{\text{TE}} \\ E_{\text{TM}} \exp(i\psi) \end{bmatrix}, \quad \text{with } E_{\text{TE}}, E_{\text{TM}} \geq 0. \tag{1}$$

We express the transmission properties of the slit as a Jones matrix. Its off-diagonal elements are zero, because the TE and TM directions are the slit's eigenpolarizations, and the diagonal elements represent the complex amplitude transmission. The output field is then the Jones vector:

$$\mathbf{E}_{\text{out}} = \begin{bmatrix} t_{\text{TE}} & 0 \\ 0 & t_{\text{TM}} \end{bmatrix} \mathbf{E}_{\text{in}}. \tag{2}$$

#154733 - $15.00 USD Received 16 Sep 2011; revised 28 Oct 2011; accepted 2 Nov 2011; published 14 Nov 2011

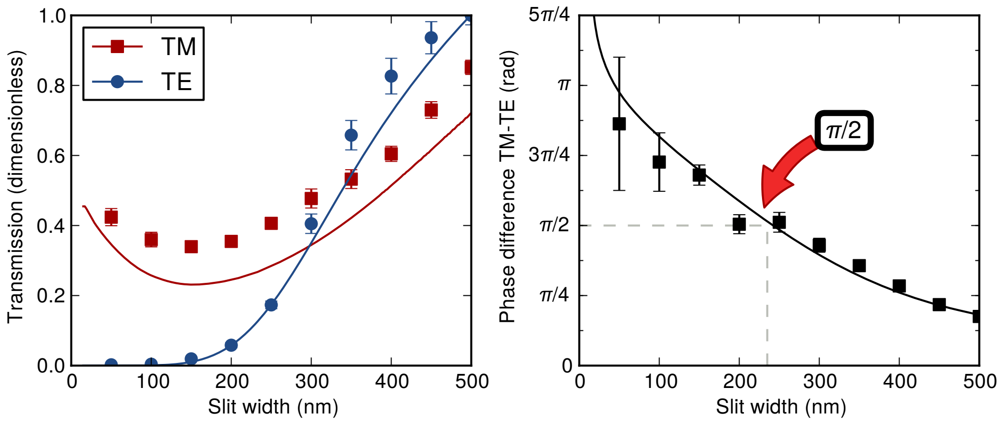

Fig. 4. (a) Dichroism of a subwavelength slit. The points show the measured transmission for TM and TE-polarized incident light as a function of the slit width w, normalized to the TE transmission at $w = 500$ nm. The solid lines show our model's result for the slit transmission. (b) Birefringence of a subwavelength slit. The points represent the measured phase difference between the TM and TE modes as a function of the slit width. They are obtained from a fit of the various Stokes parameters of Fig. 2. The solid line shows the calculated phase difference (see Eq. (9).) At a certain slit width, indicated by the arrow, the phase difference reaches $\pi/2$ and the slit acts as a quarter-wave retarder.

First, it is instructive to calculate the transmission T_{TE} and T_{TM} in order to get an idea of the slit's dichroism. Here, we define the transmission $T = |t|^2$ as the ratio of power emerging from a slit to power incident on the slit. It can be calculated from the unnormalized Stokes parameter S_1 for incident light with $s_1 = \pm 1$. T_{TE} and T_{TM} are plotted in Fig. 4a, normalized so that $T_{\text{TE}} = 1$ at $w = 500$ nm. As the slit width w is decreased, we see that the TE and TM transmission also decreases until $w \approx 350$ nm. When w is further reduced, the TM transmission goes through a minimum at $w \approx 150$ nm, where the light-surface plasmon coupling is maximum. It increases again when the slit width gets even smaller, whereas the TE transmission goes through a gradual cutoff, becoming negligible only for the narrowest slits. Apparently, a narrow slit in a *thin* metal film is not such a good polarizer as often assumed.

In order to calculate the phase lag $\Delta\phi$ between the TE and TM-polarized components of the transmitted field, we write the normalized Stokes parameters in terms of Eq. (2):

$$s_1 = -\frac{T_R E_{\text{TM}}^2 - E_{\text{TE}}^2}{T_R E_{\text{TM}}^2 + E_{\text{TE}}^2}, \tag{3}$$

$$s_2 = \frac{2T_R^{1/2} E_{\text{TM}} E_{\text{TE}}}{T_R E_{\text{TM}}^2 + E_{\text{TE}}^2} \cos(\Delta\phi - \psi), \tag{4}$$

$$s_3 = -\frac{2T_R^{1/2} E_{\text{TM}} E_{\text{TE}}}{T_R E_{\text{TM}}^2 + E_{\text{TE}}^2} \sin(\Delta\phi - \psi), \tag{5}$$

where $T_R = |t_{\text{TM}}/t_{\text{TE}}|^2$ is shorthand for the transmission ratio. We calculate $\Delta\phi$ from our measured Stokes parameters using Eqs. (3), (4), and (5). It is plotted in Fig. 4b, where we see that it decreases almost linearly with increasing slit width. It passes through a value of $\pi/2$ at $w \approx 250$ nm. Although the retardation equals $\lambda/4$, the 250 nm slit does not act as an ideal quarter-wave retarder because the amplitudes of the TE and TM-polarized components of the transmitted light are not equal, as noted earlier.

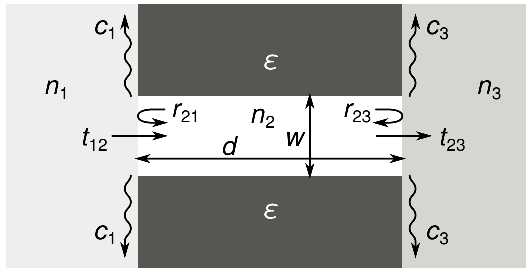

Fig. 5. Cross-section of our model slit. The relevant physical quantities are illustrated.

Figure 4a illustrates the slit's dichroism and Fig. 4b its birefringence. The effect that we observe in Fig. 2 as the slit width is decreased from 500 to 300 nm can be explained in terms of increasing birefringence and small dichroism in that range. Below 300 nm, dichroism becomes more important, and consequently, the main axis of the polarization ellipse rotates. The dichroism observed here was suggested by the simulations in Ref. [18], where ultrashort TE pulses were shown to experience lower propagation speeds through a slit in an aluminum layer. If the slit width is further decreased past the surface plasmon-induced minimum at $w \approx 150$ nm, the dichroic effect becomes even larger. The TE-polarized component of the transmitted light becomes weaker and weaker, while the TM-polarized component grows, causing the polarization ellipse to collapse to a vertical line. We see that the waveguide's TE cutoff does not resemble a sharp cutoff at $w = \lambda/2$ at all, but rather a gradual one.

4. Waveguide model

We will now proceed to explain these experimental results by modeling the slit as a simple waveguide. Our slit forms a rectangular waveguide with a large width/height ratio. For that reason we can effectively describe each slit as a step-index planar waveguide, with its walls made of a metal with relative permittivity ε. Inside the waveguide, the solutions to Maxwell's equations separate into TE and TM modes, each with a complex propagation constant β. Although the equations are exact, we must calculate the propagation constants for each mode, β_{TE} and β_{TM}, numerically [19].

Knowing that the propagation constant is equal to $k_0 = 2\pi/\lambda$ times the effective mode index allows us to calculate coupling coefficients to and from the waveguide mode. For the TM and TE modes, we calculate complex reflection and transmission coefficients r_{21}, t_{12}, r_{23}, and t_{23} using the Fresnel equations at normal incidence, substituting the effective mode index for the index of medium 2. As shown in Fig. 5, the index 1 indicates the medium from which the light is incident (air), 2 the waveguide, and 3 the medium into which the transmitted light emerges (glass in our experiment). This simplification avoids calculating overlap integrals between the guided mode and the modes outside the waveguide, but still describes the observed phenomena quite well. We can then treat the waveguide as a Fabry-Pérot interferometer and calculate each mode's complex transmission through a waveguide of length d,

$$t_{123} = \frac{t_{12}t_{23}\exp(i\beta d)}{1 - r_{21}r_{23}\exp(2i\beta d)}, \tag{6}$$

#154733 - $15.00 USD Received 16 Sep 2011; revised 28 Oct 2011; accepted 2 Nov 2011; published 14 Nov 2011

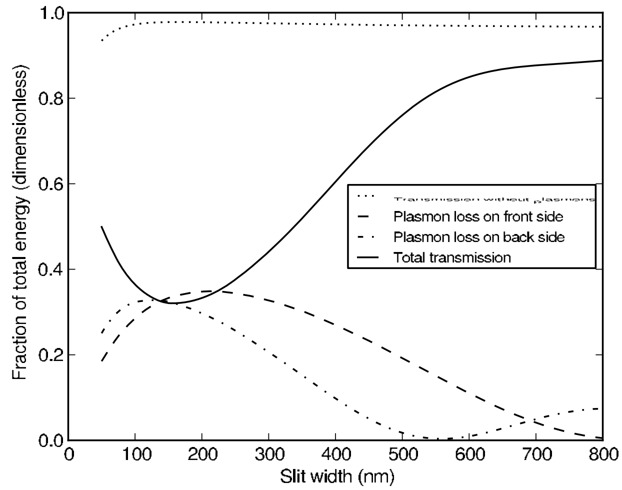

Fig. 6. Calculated effect of surface plasmons on the transmission of TM-polarized light as a function of the slit width w. The dotted line shows the calculated TM transmission neglecting any coupling to surface plasmons, based on waveguide theory alone, i.e. $(n_3/n_1)|t_{123}^{\mathrm{TM}}|^2$. The dashed line shows the total fraction of energy converted to surface plasmons on the illuminated (front) side of the sample according to Ref. [15], i.e. $2|c_1|^2$ as mentioned in Eq. (8). Likewise, the dot-dashed line shows the fraction converted to surface plasmons on the unilluminated (back) side, i.e. $2|c_3|^2$. Finally, the solid line shows the total TM transmission according to Eq. (8). In these calculations, we disregard the numerical aperture of the imaging system.

which gives for the transmission

$$T_{\mathrm{TE}} = \frac{n_3}{n_1}|t_{123}^{\mathrm{TE}}|^2, \tag{7}$$

$$T_{\mathrm{TM}} = \frac{n_3}{n_1}|t_{123}^{\mathrm{TM}}|^2 - 2|c_1|^2 - 2|c_3|^2. \tag{8}$$

Here, c_1 and c_3 are the coupling constants of the slit system to a surface plasmon mode traveling in one direction away from the slit on the interface with medium 1 or 3, as calculated from Eq. (20) of Ref. [15], which gives an approximate analytical model. As an illustration of the important role these surface plasmon coupling constants play in the phenomenon described here, the TM transmission modelled with and without coupling to surface plasmons is shown in Fig. 6. The TE mode does not couple to surface plasmons.

It is interesting to note in Fig. 6 that the surface plasmon coupling coefficients on both sides exhibit a maximum at $nw/\lambda \approx 0.23$ and a minimum at $nw/\lambda \approx 1$, as predicted by Ref. [15]. These two curves added together produce a maximum in the surface plasmon excitation, and therefore a dip in the TM transmission, at around $w \approx 150$ nm.

In our model we ignore the thin titanium adhesion layer present between the gold and the glass. According to the model, the $|c_3|$ coefficient for a thick titanium layer would be slightly higher than that of the gold layer. However, we expect that the layer is too thin to have any effect on the coupling between the slit TM mode and surface plasmons. It does not prevent the light from scattering into the surface plasmon mode, but only ensures that the surface plasmon mode is very lossy.

Nevertheless, our straightforward model exhibits good agreement with the measurements, despite the fact that it does not contain any fitting parameters. The slit's gradual TE cutoff is

#154733 - $15.00 USD Received 16 Sep 2011; revised 28 Oct 2011; accepted 2 Nov 2011; published 14 Nov 2011

predicted well, and can be ascribed to gold not being a perfect conductor at this wavelength, and to the considerable dispersion of the reflection coefficients r_{12} and r_{23} around cutoff. The model also predicts a plasmon-related TM transmission dip at the right slit width. In Fig. 4a, we compare these calculated values to our measurements. In our calculations, we took the finite numerical aperture and its influence on the TM and TE transmission into account.

The complex transmission also gives us the relative phase delay between the TM and TE modes:

$$\Delta\phi = \arg t_{123}^{\mathrm{TM}} - \arg t_{123}^{\mathrm{TE}} \pmod{2\pi}. \tag{9}$$

This phase difference is plotted in Fig. 4b and compared to the values calculated from our measurements using Eqs. (3), (4), and (5). The values predicted by our simple model for the phase delay exhibit excellent agreement with the measurements.

The model presented here suggests exploring the parameter space in order to design slits that act as non-dichroic quarter-wave retarders. The requirements are that the TM and TE transmission are equal after the TM loss to surface plasmons, and that the phase difference is $\pi/2$. All these requirements are influenced by the metal permittivity $\varepsilon(\lambda)$, the slit width w, and the film thickness d.

5. Conclusion

In summary, we have studied the transmission properties of a sub-wavelength slit milled in a 200 nm thick gold-metal film as a function of the slit width (50–500 nm), and of the polarization of the incident radiation (at $\lambda = 830$ nm). As the slit width is decreased, the transmission of the TE mode diminishes quite gradually until it becomes very small at a slit width of about $\lambda/8$, reminiscent of the phenomenon of waveguide cutoff. In contrast, the transmission of the TM mode does not vanish. Instead, it exhibits a characteristic dip at a certain slit width, associated with the efficient excitation of surface plasmons.

Moreover, we have studied the birefringence of this subwavelength slit and found that the phase lag between the TM and TE modes passes through a value of $\pi/2$, so that a properly dimensioned slit can act as a quarter-wave retarder. We have successfully explained our experimental results with a simple waveguide model.

Our experimental results contradict a recently published proposal for a quarter-wave retarder using perpendicular metallic nanoslits [20], where the width of the slits is varied purely to control the TM transmission. Varying the width of the slit also changes the TE transmission of the incident light and the phase difference between the TM and TE components.

Acknowledgments

The authors thank Dr. Wolfgang Löffler for his assistance in automating the measurement of the Stokes parameters. This work is part of the research program of the Foundation for Fundamental Research on Matter (FOM), which is part of the Netherlands Organisation for Scientific Research (NWO).